# Nuclear pore complexes undergo Nup221 exchange during blood stage asexual replication of *Plasmodium* parasites.

**Authors:**

James Blauwkamp[1]*, Sushma V Ambekar[2]*, Tahir Hussain[2], Gunnar R Mair[2,3#], Josh R. Beck[2#], Sabrina Absalon[1#]

**Affiliations:**

[1]Indiana University School of Medicine, Department of Pharmacology and Toxicology

[2]Iowa State University, Department of Biomedical Sciences

[3]School of Biological Sciences, Queen's University Belfast

*These authors contributed equally

[#]Co-corresponding Authors

Co-Corresponding Authors Email:

g.mair@qub.ac.uk

jrbeck@iastate.edu

sabsalon@iu.edu

**Summary Statement:**

Employing ultrastructure expansion microscopy and the RITE system, this study unveils Nup221 turnover in nuclear pore complexes of *Plasmodium* parasites, shedding light on their replication mechanisms.


## Abstract

*Plasmodium* parasites, the causative agents of malaria, undergo closed mitosis without breakdown of the nuclear envelope. Unlike closed mitosis in yeast, *P. berghei* parasites undergo multiple rounds of asynchronous nuclear divisions in a shared cytoplasm which results in a multinucleated organism prior to formation of daughter cells within an infected red blood cell. During this replication process, intact nuclear pore complexes (NPCs) and their component nucleoporins play critical roles in parasite growth, facilitating selective bi-directional nucleocytoplasmic transport and genome organization. Here we utilize ultrastructure expansion microscopy (U-ExM) to investigate *P. berghei* nucleoporins at the single nucleus level throughout the 24-hour blood-stage replication cycle. Our findings reveal that these Nups are evenly distributed around the nuclei and organized in a rosette structure previously undescribed around the centriolar plaque, which is responsible for intranuclear microtubule nucleation during mitosis. By adapting the recombination-induced tag exchange (RITE) system to *P. berghei*, we provide evidence of NPC maintenance, demonstrating Nup221 turnover during parasite asexual replication. Our data shed light on the distribution of NPCs and their homeostasis during the blood-stage replication of *P. berghei* parasites.

49 **Introduction:**

50 The survival and growth of eukaryotic organisms relies on the movement of
51 macromolecules between the membrane bound nucleus and the cytosol. This nuclear-cytosolic
52 transport is facilitated by nuclear pore complexes (NPCs) that are embedded into the nuclear
53 envelope. Apart from being a channel for selective bidirectional nucleocytoplasmic transport, the
54 NPC plays a key role in chromatin organization, gene regulation, DNA repair, and maintenance of
55 epigenetic memory in many eukaryotes (Lin and Hoelz 2019). Typically, these NPCs are composed
56 of multiple copies of more than 30 different nucleoporins (Nups) per NPC, with eukaryotic NPCs
57 containing around 1000 proteins total (Hoelz, Debler et al. 2011, Grossman, Medalia et al. 2012,
58 Ori, Banterle et al. 2013, Otsuka and Ellenberg 2018, Lin and Hoelz 2019). Nups are widely
59 conserved in most eukaryotes, including yeasts, humans, and various plant species, and have also
60 been identified in parasitic protozoa such as *Trypanosoma brucei* and *Toxoplasma gondii*
61 (Degrasse and Devos 2010, Courjol, Mouveaux et al. 2017). Nups are separated into two distinct
62 categories; structural Nups that form the pore and the intrinsically disordered phenylalanine-
63 glycine repeat (FG) Nups which regulate nucleocytoplasmic transport (Fig. 1a) (Devos,
64 Dokudovskaya et al. 2006, Beck and Hurt 2017). Structurally, the NPCs establish an inner channel
65 called the inner ring, flanked by the outer rings on the cytosolic and nuclear side of the NPC. After
66 the inner channel is constructed the cytoplasmic filament and the nuclear basket Nups attach to
67 their appropriate side of the pore (Devos, Dokudovskaya et al. 2006, Beck and Hurt 2017). The FG
68 Nups, characterized by their FG repeats, occupy the space inside the inner ring and interact with
69 the cargo to facilitate nuclear-cytosolic transport (Strawn, Shen et al. 2004, Devos, Dokudovskaya
70 et al. 2006, Beck and Hurt 2017).

71 One of the most extensively studied organisms with respect to the dynamics and
72 structural aspects of nuclear pore complexes is budding yeast. *Saccharomyces cerevisiae*
73 undergoes closed mitosis during which the nuclear envelope remains intact during karyokinesis.
74 In contrast to open mitosis, where NPC removal during prophase leads to nuclear envelope
75 breakdown, in closed mitosis it has been hypothesized that specific regions of nuclear pore/
76 complex disassembly cause small breaks in the nuclear envelope, facilitating nuclear envelope
77 fission and formation of two new nuclei (Lénárt, Rabut et al. 2003, Dey, Culley et al. 2020). Like

78 budding yeast, the parasites of the *Plasmodium* genus, the causative agent of malaria, undergo a
79 specialized form of closed mitosis. In these parasites, multiple rounds of asynchronous nuclear
80 division in a shared cytoplasm leads to a multinucleated single-celled parasite (Gerald, Mahajan
81 et al. 2011). While many Nups are conserved through eukaryotes, *Plasmodium* Nups are very
82 divergent, which makes their identification by bioinformatics challenging. In a 2010 study aiming
83 to identify Nups of different eukaryotes, only two Nups were identified in *P. berghei* compared to
84 19 identified Nups in over 50 different organisms (Neumann, Lundin et al. 2010). Eleven Nups are
85 currently known in the rodent malaria model *P. berghei*; Sec13. Five FG Nups, and five novel Nups
86 identified using Nup313 as bait in proximal labeling assays (Fig. 1a) (Dahan-Pasternak, Nasereddin
87 et al. 2013, Kehrer, Kuss et al. 2018, Ambekar Sushma, Beck Josh et al. 2022). Interestingly, only
88 one of these proteins presents established structural features of eukaryotic Nups (Beck and Hurt
89 2017).

90 The limited understanding of essential components of nuclear pore complexes in
91 *Plasmodium* is attributed to the absence of protein homology for Nup identification in
92 *Plasmodium* and the lack of suitable tools to investigate the dynamics of NPCs within relatively
93 small nuclei (a micrometer). While conventional fluorescence and electron microscopy
94 techniques have provided valuable insights into the perinuclear localization of identified Nups in
95 *Plasmodium* parasites, these approaches suffer from low resolution and the significant financial
96 and time investments required for electron microscopy (Doye, Wepf et al. 1994, Winey, Yarar et
97 al. 1997, Weiner, Dahan-Pasternak et al. 2011, Colombi, Webster et al. 2013, Beck and Hurt 2017,
98 Kehrer, Kuss et al. 2018, Dey, Culley et al. 2020, Bertiaux, Balestra et al. 2021). These challenges
99 in comprehending the dynamics and distribution of nuclear pore complexes (NPCs) in
100 *Plasmodium* parasites have spurred the exploration of innovative microscopy techniques to
101 overcome these limitations and gain deeper insights into these vital components. The adaptation
102 of Ultrastructure Expansion Microscopy (U-ExM) to work with parasites now allows for super-
103 resolution imaging of parasites in a cost-effective and high-throughput manner (Gambarotto,
104 Zwettler et al. 2019, Caroline, Charlotta et al. 2021, Liffner and Absalon 2021, Liffner, Cepeda Diaz
105 et al. 2023). U-ExM achieves isotropic expansion of biological samples, increasing their size up to
106 4.5 times by embedding denatured samples into a hydrogel that expands when exposed to water.

107 Notably, this technique has been employed to achieve sub-nucleus resolution and has
108 successfully visualized Nup313 at the nuclear membrane in *P. falciparum* (Caroline, Charlotta et
109 al. 2021, Liffner, Cepeda Diaz et al. 2023).

110 In this study, we employed U-ExM to visualize individual NPCs using tagged versions of *P.*
111 *berghei* Nup138, Nup221, and Nup313. We successfully localized these Nups to the nuclear
112 envelope by employing NHS ester or BodipyFL Ceramide staining throughout the asexual life cycle
113 of the *P. berghei* parasite. Consistent with prior findings using "serial surface" imaging in focused
114 ion beam – scanning electron microscopy (FIB-SEM)(Weiner, Dahan-Pasternak et al. 2011), we
115 observed an increase in NPC number until the parasite's first mitosis, during which the NPCs were
116 then distributed between the newly developing nuclei. We proceeded to assess NPC assembly
117 and protein turnover using the Recombination Induced Tag Exchange (RITE) system marking the
118 first time this has been accomplished in *Plasmodium*. The RITE system uses a conditional,
119 hormone activated Cre-recombinase to generate permanent epitope tag switch in a target coding
120 sequence. This method has been previously utilized in human cells to observe the dynamic
121 replacement of NPC components in human neurons (Verzijlbergen, Menendez-Benito et al. 2010,
122 Toyama, Arrojo e Drigo et al. 2018).

123 Leveraging the enhanced resolution of U-ExM coupled with the RITE system, we were able
124 to monitor NPC assembly and maintenance dynamics within a single nucleus during *Plasmodium*
125 replication. In line with previous observations in mammalian cells, we found that NPCs in *P.*
126 *berghei* undergo protein maintenance after the NPCs have been produced. Remarkably, we also
127 confirmed the presence of Nup221 proteins of different ages in a single NPC by colocalization of
128 original and induced Nup221 signal. Our results expand upon existing data and showcase the new
129 insights achievable through the combination of U-ExM with genetic and biochemical systems.

130 **Results:**

131 **U-ExM visualization of Nups around the nucleus.**

132 Previous studies on NPCs in various organisms have predominantly relied on slide-based
133 immunofluorescence assays. For higher resolution, NPCs could be visualized by electron
134 microscopy, but this process is time consuming and costly. The emergence of expansion

135 microscopy in smaller organisms like yeast has significantly advanced NPC visualization and study
136 (Hinterndorfer, Laporte et al. 2022). In our efforts to visualize nucleoporins (Nups) at single NPC
137 resolution in *P. berghei*, we introduced C-terminal endogenous epitope tags on three previously
138 identified *P. berghei* FG Nups: spaghetti monster Hemagglutinin (smHA) tags on Nup138 and
139 Nup313 and a 3xHA/GFP tag on Nup221 (Fig. 2). In comparison to previous studies on
140 unexpanded parasites (Kehrer, Kuss et al. 2018, Ambekar Sushma, Beck Josh et al. 2022), and
141 considering the expected size of the NPCs in yeast (Hinterndorfer, Laporte et al. 2022), expansion
142 microscopy successfully resolves individual NPCs around the nuclear periphery (Fig. 1b). To
143 confirm the position of these Nups at the nuclear membrane, we employed different approaches,
144 visualizing the nuclear membrane using an endoplasmic reticulum (ER) antibody (PfBIP),
145 employing membrane stains such as Bodipy TR Ceramide and Bodipy FL Ceramide, and assessing
146 membrane localization through NHS Ester staining variations around the nucleus (Fig. S1). Among
147 these methods, we determined that differences in NHS ester staining and high concentrations of
148 Bodipy FL Ceramide effectively delineated the nuclear envelope to confidently assign the NPC
149 signal to this structure. In summary, U-ExM allows us to observe individual NPCs on the nuclear
150 envelope.

151 ***Plasmodium berghei* produces NPCs primarily before mitosis**.

152 We next wanted to quantify the number of NPCs surrounding each nucleus during various
153 stages of the parasite's intraerythrocytic development cycle. To achieve this, we performed U-
154 ExM on parasites that exhibited a range of nuclear numbers and were stained for either
155 Nup138::smHA or Nup313::smHA. In the early stages of the parasite's life cycle, before the
156 parasites begin their mitotic phase (1n, Ring), we observed Nup138 being uniformly distributed
157 around the nucleus (Fig. 3a), while the Nup313 signal is concentrated at either end of the nucleus
158 (Fig. S2). At this stage, we noticed a higher number of Nup313 foci (approximately 40-50 NPCs)
159 compared to Nup138 (around 25-35 NPCs) (Fig. 3b). As the parasites began mitosis (1n,
160 Trophozoite premitotic and mitotic), there was a significant 5-fold increase in both Nup138 and
161 Nup313 numbers. The parasites produce over 250 NPCs containing Nup313 and over 150 NPCs
162 containing Nup138, distributed around the single nucleus (Fig. 3b). As more nuclei are formed (2-
163 4n Schizont, 5-9n Schizont, 10+n Cytokinesis), the number of NPCs around each nucleus

164 decreased. Initially, approximately 250 NPCs surrounded a single nucleus, which then reduced to
165 around 90-100 NPCs around each of the 2 or 3 nuclei. Eventually, the count further decreases to
166 approximately 25-30 NPCs around 10-12 nuclei (Fig. 3b). Our data suggests that NPC production
167 peaks before mitosis and NPCs are then distributed during each karyokinesis.

168 ***Plasmodium berghei* NPCs are organized around the centriolar plaque.**

169 During and after the first mitosis we observe a uniform distribution of NPCs around
170 individual nuclei, as visualized by Nup138 and Nup313 (Fig. 3). Interestingly, upon the first round
171 of mitosis we detect 4-10 foci of Nup138, Nup313, and Nup221, the homolog to yeast Nup100,
172 localizing around the centriolar plaque (CP), which is the nuclear microtubule organization center
173 responsible for intranuclear microtubule nucleation (Fig. 4a)(Arnot, Ronander et al. 2011, Simon,
174 Funaya et al. 2021, Liffner, Cepeda Diaz et al. 2023). Quantification of NPCs around the centriolar
175 plaque reveals a higher count of Nup313 compared to the other two FG Nups used in this study
176 (Fig. 4b). It is important to highlight that after parasite cytokinesis, the centriolar plaque
177 disassembles (Liffner, Cepeda Diaz et al. 2023), but NPCs retain a rosette formation in the vicinity
178 of the former plaque location (Fig. 4c).

179 **The RITE system reveals NPC assembly and maintenance.**

180 NPCs in yeast undergo degradation and replacement of Nups and full NPCs (Allegretti,
181 Zimmerli et al. 2020, Lee, Wilfling et al. 2020, Tomioka, Kotani et al. 2020), and that Nup
182 replacement occurs in non-dividing human cells (Toyama, Arrojo e Drigo et al. 2018). Therefore,
183 in order to assess the turnover of Nups in *Plasmodium*, we adapted the Recombination Induced
184 Tag Exchange (RITE) system for the first time in these parasites. The RITE system uses a
185 constitutively expressed Cre recombinase fused to the human estrogen binding domain (EBD)
186 which retains the protein in the cytoplasm by association with HSP70. Upon the addition of β-
187 estradiol, Cre-EBD translocates to the nucleus where it triggers a permanent genetic switch
188 through a recombination event between two *LoxP* flanking the initial tag, removing this tag and
189 bringing a distinct tag into frame (Verzijlbergen, Menendez-Benito et al. 2010) (Fig. S3a). Here we
190 tagged *P. berghei* Nup221 with a RITE system cassette, which includes a 3xHA/GFP tag, a
191 3xMyc/RFP tag, and the two *LoxP* sites for tag switching (Fig. 2a, 5a). We found that adding as

192 little as 2 nM β-estradiol resulted in a partial switch from HA to Myc tag, while 200 nM β-estradiol
193 induces sufficient relocation into the nucleus for a complete switch from HA to Myc tag in as little
194 as 2 hours, confirmed by PCR analysis (Fig. S3b, c).

195 Initial immunofluorescence imaging over the course of a 16-hour period for both control
196 and 200 nM β-estradiol treated parasites showed visible tag switching by eight hours post
197 induction with β-estradiol (Fig. S4a). By the end of the 16-hour period we observed individual
198 parasites (merozoites) that expressed a mixture of Nup221 tagged with GFP or RFP, both in a
199 typical polar localization. By PCR genotyping, we can detect tag exchange within two hours of
200 estrogen addition. Notably, the continued detection of Nup221-HA through 16 hours post
201 induction indicates a stable population of Nup221 persists for at least eight hours during the
202 parasite life cycle (Fig. S4). To validate complete turnover of Nup221 and ensure no spurious
203 excision was occurring, samples from control and induced conditions were allowed to propagate
204 for an additional 96 hours (four parasite development cycles). While Myc-tagged Nup221 was
205 never detected in control samples, HA-tagged Nup221 was no longer detectable in β-estradiol
206 treated parasites after 96 hours. These results demonstrate that the RITE system is an effective
207 tool for monitoring Nup221 turnover in *P. berghei.* Pairing this technique with U-ExM will provide
208 better resolution for determining NPC maintenance in the parasites.

209 ***Plasmodium berghei* replaces Nups in post-mitotic NPCs.**

210 To investigate NPC assembly and maintenance during and after mitosis, we treated newly
211 invaded parasites (1N) with 200 nM β-estradiol and cultured for 20 hours. We then collected
212 processed samples for U-ExM at 0, 10, and 20 hours post induction with β-estradiol to determine
213 Nup221 presence in NPCs before mitosis occurs (10 hours post induction) and after mitosis,
214 during cytokinesis (20 hours post induction). We hypothesized that if Nup221 is being replaced in
215 the post-mitotic NPCs, we would observe a signal shift from the original HA signal (pink) to the
216 induced Myc signal (yellow), with a higher proportion of induced signal in the 20 hours post
217 induction samples.

218 At 0 hours post induction, early-stage parasites display only the original HA signal (Fig. 5b).
219 At 10 hours post induction, parasites mature and undergo the first rounds of mitosis resulting in

220 the formation of 2-3 nuclei. These parasites exhibit a mix of the HA and Myc signals, with 50% of
221 foci containing only HA signal, 35% of foci containing only Myc signal, and 15% of foci containing
222 both the HA and Myc signals (Fig. 5b, c). The presence of co-localized HA and Myc signals suggests
223 multiple copies of Nup221 in individual NPCs. By 20 hours post induction with β-estradiol the
224 parasites have stopped producing new NPCs. At this time we found 35% of NPCs contain only HA
225 signal, while 50% of NPCs contain only Myc signal and 15% of NPCs contain both HA and Myc
226 signal (Fig. 5b, c). This result suggests novel Nup221-Myc incorporation into existing NPCs after
227 the parasites have stopped producing them.

228 Subsequently, we wondered whether the Nups in the NPCs around the CP were subjected
229 to maintenance at the same rate as those around the nuclei. To test this, we specifically
230 monitored the turnover of Nup221 within the NPCs surrounding the CP. At 0 hours post induction,
231 when no CPs are visible, Nup221 is evenly distributed around the parasite nucleus. By 10 hours
232 post induction the CP is present, and now 50% of the NPCs surrounding it contained only the
233 original signal, mirroring observations around the rest of the nucleus. Around 20% of the NPCs
234 contain only the induced signal, a decrease of 15% compared to around the ones around the
235 nucleus, and 30% of the NPCs contain both the original and induced signal, an increase of 15%
236 compared to those scattered around the nucleus (Fig. 5d). This suggests that the turnover of the
237 original Nup221 signal occurs at a slower pace in the NPCs surrounding the nucleus compared to
238 those scattered around it. This trend persists at 20 hours post induction, where 30% of NPCs
239 showed only the original signal, similar to what was seen around the rest of the nucleus. However,
240 45% of the NPCs contain only the induced signal (a decrease from 50%) and 25% of the NPCs
241 contain both the original and induced signal (an increase from 15%) (Fig. 5d). Altogether, our data
242 indicate that proteins in the NPCs surrounding the CP exhibit greater stability than those in NPCs
243 scattered around the nucleus.

244 **Discussion**

245 In this study, we applied U-ExM and the RITE System to investigate the distribution and
246 homeostasis of NPCs in the asexual blood stages of the rodent malaria model, *P. berghei*. Previous
247 work on Nups in *Plasmodium* presented challenges due to both the divergent nature of the Nups

248 and the relatively small size of the parasite nucleus at approximately 1 µm. Our results
249 demonstrate the effectiveness of U-ExM in resolving individual NPCs around the parasite nucleus,
250 enabling us to address questions about their individual characteristics. Additionally, for the first
251 time we adapted the RITE system in *Plasmodium,* allowing us to dissect the mechanisms of NPC
252 maintenance. While the RITE system was employed here to monitor protein turnover by tag
253 exchange, it should also be amenable to other conditional mutagenesis strategies, providing an
254 alternative conditional excision strategy in addition to the established dimerizable Cre (DiCre)
255 system (Kent, Modrzynska et al. 2018, Fernandes, Briquet et al. 2020), expanding the genetic
256 toolkit in this important rodent malaria model.

257 This study defined the number of Nups surrounding the nucleus during the asexual life
258 cycle of *P. berghei*, unraveling a dual localization of NPCs around individual nuclei. Interestingly,
259 we observed a rosette structure around the centriolar plaque (CP) during nuclear replication and
260 this NPC organization persisted in merozoites even when the CP was no longer visible. Our
261 findings align with Ferreira et al, using CryoEM to examine microtubules in *P. falciparum* parasites,
262 revealing a similar ordered NPC structure around the CP during mitosis (Ferreira, Pražák et al.
263 2023). This circular organization, previously unreported and not observed outside of *Plasmodium*,
264 could suggest a specific role of these NPCs in CP formation, duplication, maintenance, and
265 function during mitosis. For example, *S. cerevisiae* NPC protein Ndc1, a subunit of the
266 transmembrane ring, is a key protein in inserting the nuclear MTOC into the nuclear envelope
267 (Chial, Rout et al. 1998, Jaspersen and Ghosh 2012).

268 By quantifying individual Nup foci around the nuclei, we determined the number of NPCs
269 per nucleus throughout the life cycle. Our results indicate a rapid increase in NPCs just before the
270 first round of mitosis, consistent with previous observations *in P. falciparum* (Weiner, Dahan-
271 Pasternak et al. 2011). The higher NPC count observed in our study (250 vs 60) might be attributed
272 to greater sample numbers achievable with U-ExM compared to FIB-SEM (our data was taken
273 from 150+ nuclei from 60+ cells over two biological samples) and improved NPC detection by
274 immunostaining against the endogenously tagged Nups.

275 Previous research in various cell types has shown that the composition of NPCs at specific
276 stages in the cell cycle can influence cell fate (Kane, Rebensburg et al. 2018, Gomar-Alba and
277 Mendoza 2020). In *Plasmodium* parasites it has been shown that SEC13, a component of the
278 nuclear pore complexes and the COPII coat, show a different localization than FG Nups (Kehrer,
279 Kuss et al. 2018). Our study delved into the heterogeneity of NPCs by examining three FG-Nups:
280 Nup138, Nup221 and Nup313. Notably, Nup313 showed a distinct localization in the early ring
281 stage of the parasite suggesting a potential specialized role during this stage of development.
282 Further investigations into the dynamic localization of different types of Nups would be
283 interesting to assess whether Nup313's temporal differential localization is unique or shared with
284 other Nups that compose the NPC.

285 Our data indicate that most NPCs contain a single version of Nup221, whether pre-mitotic
286 (Fig. 5c – Nup221-HA, pink) or post-mitotic (Fig. 5c – Nup221-Myc, yellow). However, some NPCs
287 exhibited both pre- and post-mitotic proteins, suggesting a gradual turnover in response to
288 protein degradation or damage (Fig. 5c). These observations echoed findings using the RITE
289 system by Toyama et al., suggesting an active mechanism for NPC maintenance in mammalian
290 cells (Toyama, Arrojo e Drigo et al. 2018). This could also point towards the octagonal rotational
291 symmetry that has been seen in other organisms (Unwin and Milligan 1982, Hinshaw and Milligan
292 2003). Interestingly, we note a slight increase in protein stability around the CPs, illustrated by
293 higher colocalization between Nup221-HA and Nup221-Myc proteins than around the rest of the
294 nucleus (Fig. 5d), suggesting a higher longevity of this FG Nup in NPCs rosette compared to those
295 scattered across the nucleus.

296 With the identification of numerous Nups in the *Plasmodium* genome (Kehrer, Kuss et al.
297 2018, Ambekar Sushma, Beck Josh et al. 2022), and improved tools for visualizing NPCs, we are
298 now poised to investigate the individual functions of Nups. While the exact roles of specific Nups
299 in the *Plasmodium* parasites remains unknown, studies in other organisms have illuminated the
300 involvement of FG Nups in various cellular processes such as protein synthesis (Pulianmackal,
301 Kanakousaki et al. 2022), NPC localization and composition (Wu, Kasper et al. 2001, Ferreira, Stear
302 et al. 2017), as well as RNA transport (Powers, Forbes et al. 1997, Courjol, Mouveaux et al. 2017).
303 While no studies of specific FG Nup function have been conducted in *Plasmodium* parasites,

304 deletions of Nup138 and Nup221 in genome wide screens and individual knock-out attempts have
305 shown all Nups to be essential (Gomes, Bushell et al. 2015, Bushell, Gomes et al. 2017, Zhang,
306 Wang et al. 2018). Likewise, partial knockdown of the Nup SEC13 in human malaria slows growth
307 of the parasite in the blood (Dahan-Pasternak, Nasereddin et al. 2013), while a C-terminal proline
308 enriched sequence from SEC13 in mouse malaria models is required for parasite growth (Kehrer,
309 Kuss et al. 2018). Thus, it is likely that disruption of Nups can lead to growth delays and impaired
310 cell viability in malaria parasites. Our work, along with prior studies, lays the foundation for future
311 research into these divergent Nups as techniques for efficient knockdown continue to advance in
312 malaria parasites.

313 One of the hallmarks of nuclear envelope breakdown in mammalian open mitosis is the
314 disassembly of NPCs following mitotic kinase signaling (Linder, Köhler et al. 2017, Dey and Baum
315 2021). This disassembly is a decisive step where multiple Nups are phosphorylated and
316 sequestered to be used upon nuclear envelope reassembly (Kutay, Jühlen et al. 2021). In contrast,
317 *Plasmodium* parasites, like yeast, undergo closed mitosis, where the nuclear envelope remains
318 intact during nuclear division (Gerald, Mahajan et al. 2011). Recent work in fission yeast has used
319 confocal microscopy (Dey, Culley et al. 2020) and expansion microscopy (Hinterndorfer, Laporte
320 et al. 2022) to look at the distribution and dynamics of NPCs in a closed mitosis model. These
321 studies identified NPCs at the bridge between dividing nuclei before nuclear envelope fission. The
322 authors hypothesize that through currently unknown mechanisms, NPC disassembly in the bridge
323 between dividing nuclei contributes to nuclear envelope disassembly, enabling nuclear division.
324 While we observed instances of dividing nuclei with a cluster of NPCs along this bridge, further
325 investigation is needed to explore this mechanism in *Plasmodium* parasites. Identification and
326 characterization of a cytoplasmic facing Nup will allow for this hypothesis to be studied further,
327 and potentially probe into the mechanisms that determine where NPC disassembly occurs and
328 its link to nuclear fission.

329 In conclusion, our study provides novel insights into the distribution, homeostasis, and
330 homogeneity of NPC complexes in *P. berghei* throughout the asexual life cycle. Understanding the
331 dynamics of these essential components is crucial, as NPCs play a vital role in parasite survival.
332 The methodologies employed here pave the way for further in-depth investigations into the

333 functions of these divergent complexes, facilitating a comprehensive understanding of their role
334 in *Plasmodium* biology. This study sets the stage for future investigations into the diverse Nups in
335 the *Plasmodium* genome and their individual functions. Disruption of Nups, whether structural
336 or FG Nups, likely impacts cell growth and viability in malaria parasites, as observed in related
337 studies. As techniques for knockdown efficiency improvement continue to evolve, exploring the
338 specific functions of Nups in *Plasmodium* is imminent.

339

340

341

342

343

344

345

346

347

348

349

350

351

352

353

354

355

356 **Figures:**

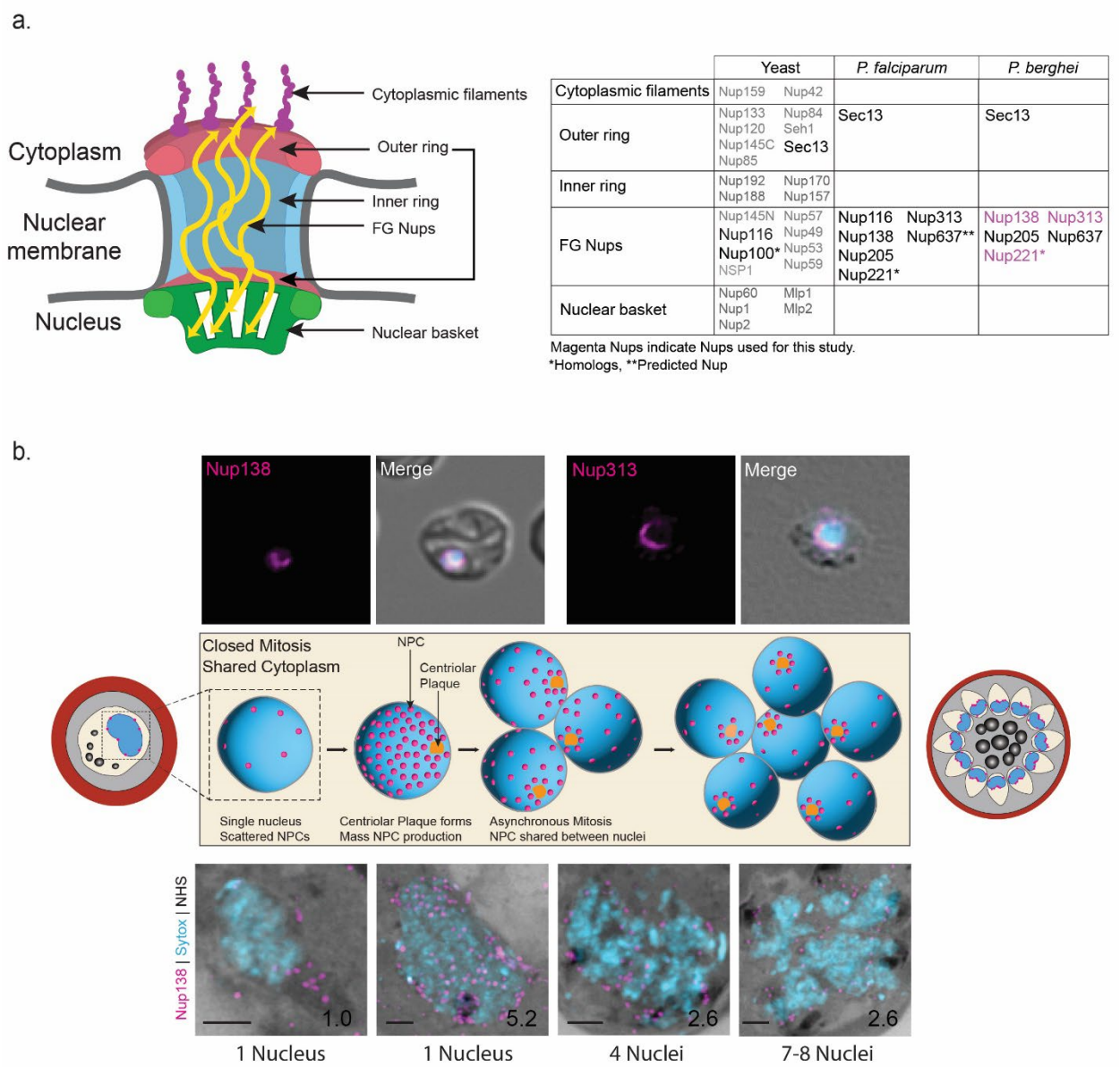


| | Yeast | | P. falciparum | | P. berghei | |
|---|---|---|---|---|---|---|
| Cytoplasmic filaments | Nup159 | Nup42 | | | | |
| Outer ring | Nup133<br>Nup120<br>Nup145C<br>Nup85 | Nup84<br>Seh1<br>Sec13 | Sec13 | | Sec13 | |
| Inner ring | Nup192<br>Nup188 | Nup170<br>Nup157 | | | | |
| FG Nups | Nup145N<br>Nup116<br>Nup100*<br>NSP1 | Nup57<br>Nup49<br>Nup53<br>Nup59 | Nup116<br>Nup138<br>Nup205<br>Nup221* | Nup313<br>Nup637** | Nup138<br>Nup205<br>Nup221* | Nup313<br>Nup637 |
| Nuclear basket | Nup60<br>Nup1<br>Nup2 | Mlp1<br>Mlp2 | | | | |

Magenta Nups indicate Nups used for this study.
*Homologs, **Predicted Nup

357

358 **Fig. 1: Divergent *P. berghei* NPCs can be analyzed by ultrastructure expansion microscopy (U-**
359 **ExM)**. **a.** Schematic representation and table of known nucleoporins (Nups) in yeast, *P.*
360 *falciparum*, and *P. berghei*. Nups highlighted in magenta indicate Nups visualized in this study,
361 Nups marked with an asterisk represent homologs, Nup637 predicted Nup. **b.** Schematic
362 representation of the *P. berghei* life cycle inside of host red blood cells, showing NPC distribution.
363 Parasites begin with a single nucleus that undergoes mitosis midway through the life cycle.
364 Multiple rounds of asynchronous mitosis lead to a multinucleated parasite with a single

365 cytoplasm before a shared cytokinetic event produces individual parasites. Also shown are
366 comparisons between unexpanded and U-ExM images of Nup138-smHA and Nup313-smHA
367 (magenta) through the life cycle showing differences in these microscopy techniques. Under the
368 U-ExM images lists the number of nuclei in the parasites shown. Scale bars 2 µm, number on
369 images indicates image depth in µm.

370

371

372

373

374

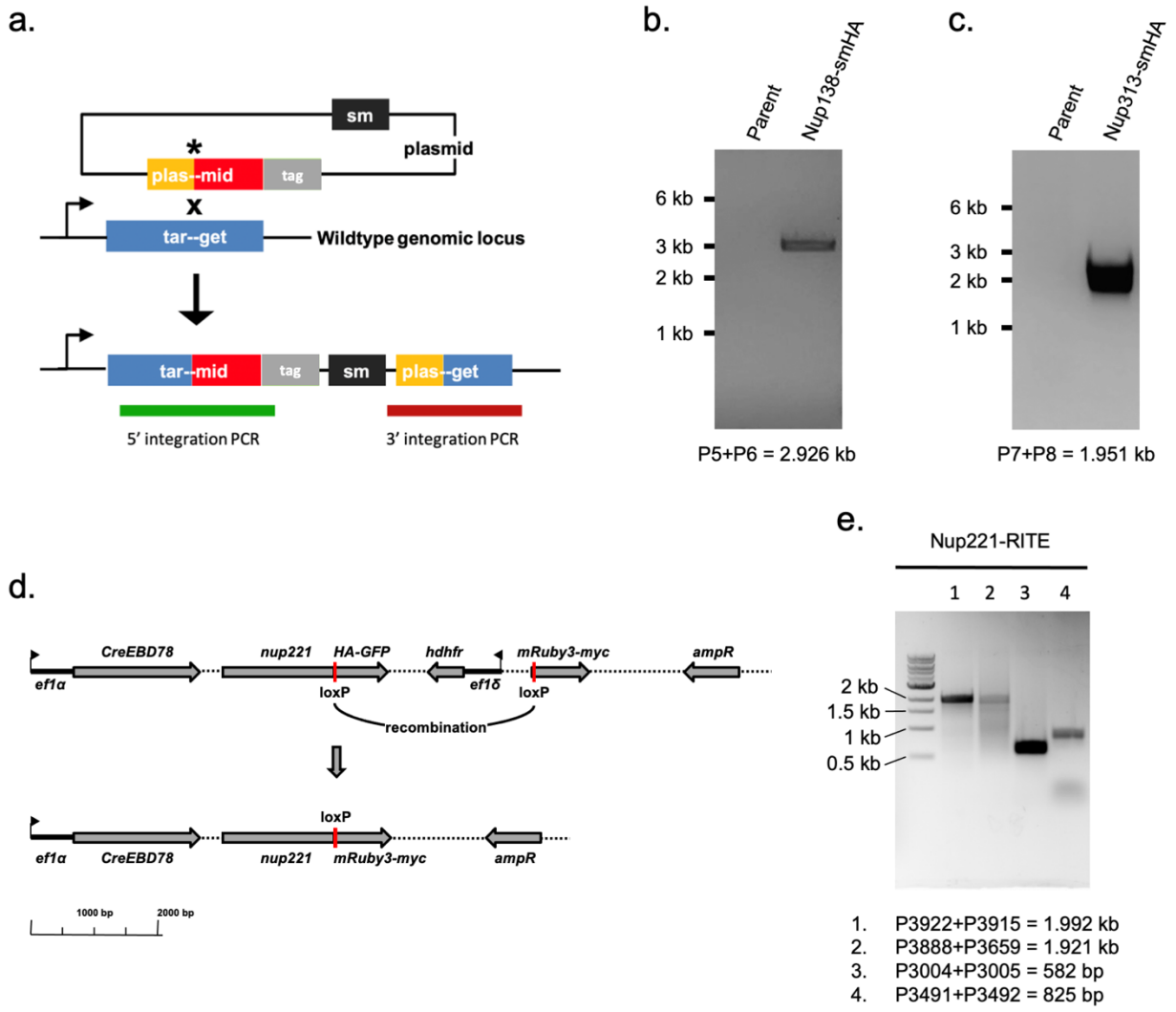


**Fig. 2: Genotyping of Nup138, Nup313 and Nup221 endogenously tagged parasite lines. a.** Schematic of general strategy for integration into the endogenous Nup138, Nup313 and Nup221 loci to generate C-terminal tag fusions. The plasmid is linearized with the homology flank targeting each gene (yellow/red box). Following transfection, homologous recombination into the target locus (blue box) results in fusion of the tag to the 3' end of the gene. Green and red lines show integration PCR products diagnostic for the successful integration. sm, selectable marker. **b,c.** 5' integration PCRs for Nup138-smHA and Nup313-smHA parasites. **d.** Schematic of the plasmid used to generate the Nup221-RITE parasites. Cre-mediated recombination between loxP sequences removes the 3xHA-GFP tag and hDHFR selection marker and brings the mRuby3-3xMyc tag into frame. **e.** Integration PCRs for the Nup221-RITE parasites. Reactions 1 and 2 are

386 diagnostic for successful 5’ and 3’ integration, respectively. Reactions 3 and 4 are controls
387 amplifying an internal portion of the plasmid and an unrelated genomic locus, respectively.

388

389

390

391

392

393

394

395

396

397

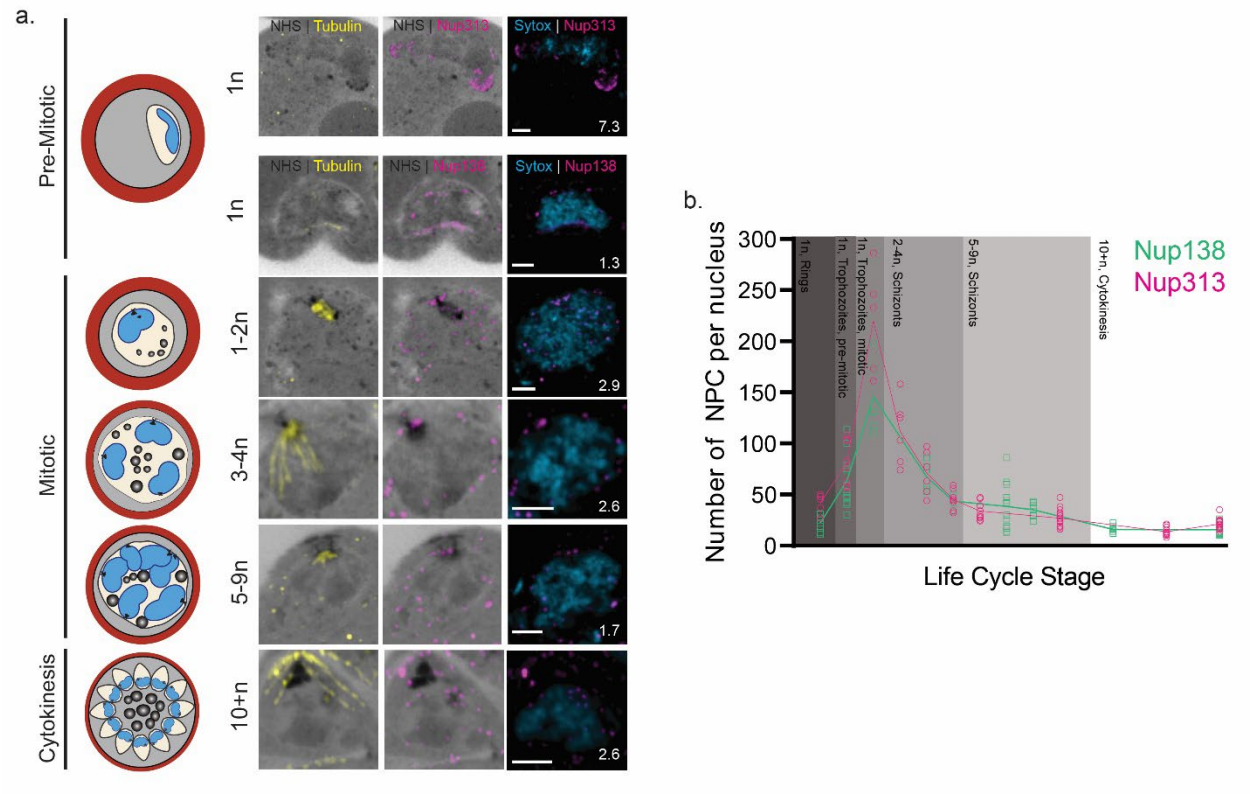


**Fig. 3: *P. berghei* produces NPCs until mitosis, distributing them among replicated nuclei.**

**a.** U-ExM images showing Nup313-smHA at early stages and Nup138-smHA through the life cycle of *P. berghei*. Microtubules shown in yellow, Nup138-smHA shown in magenta, DNA shown in blue, and protein density shown in grayscale. Scale bars 2 µm, image depth in µm indicated. **b.** Number of NPCs per nucleus through the *P. berghei* life cycle calculated by counting Nup138-smHA and Nup313 signal. Green indicates Nup138 signal and magenta indicates Nup313-smHA signal.

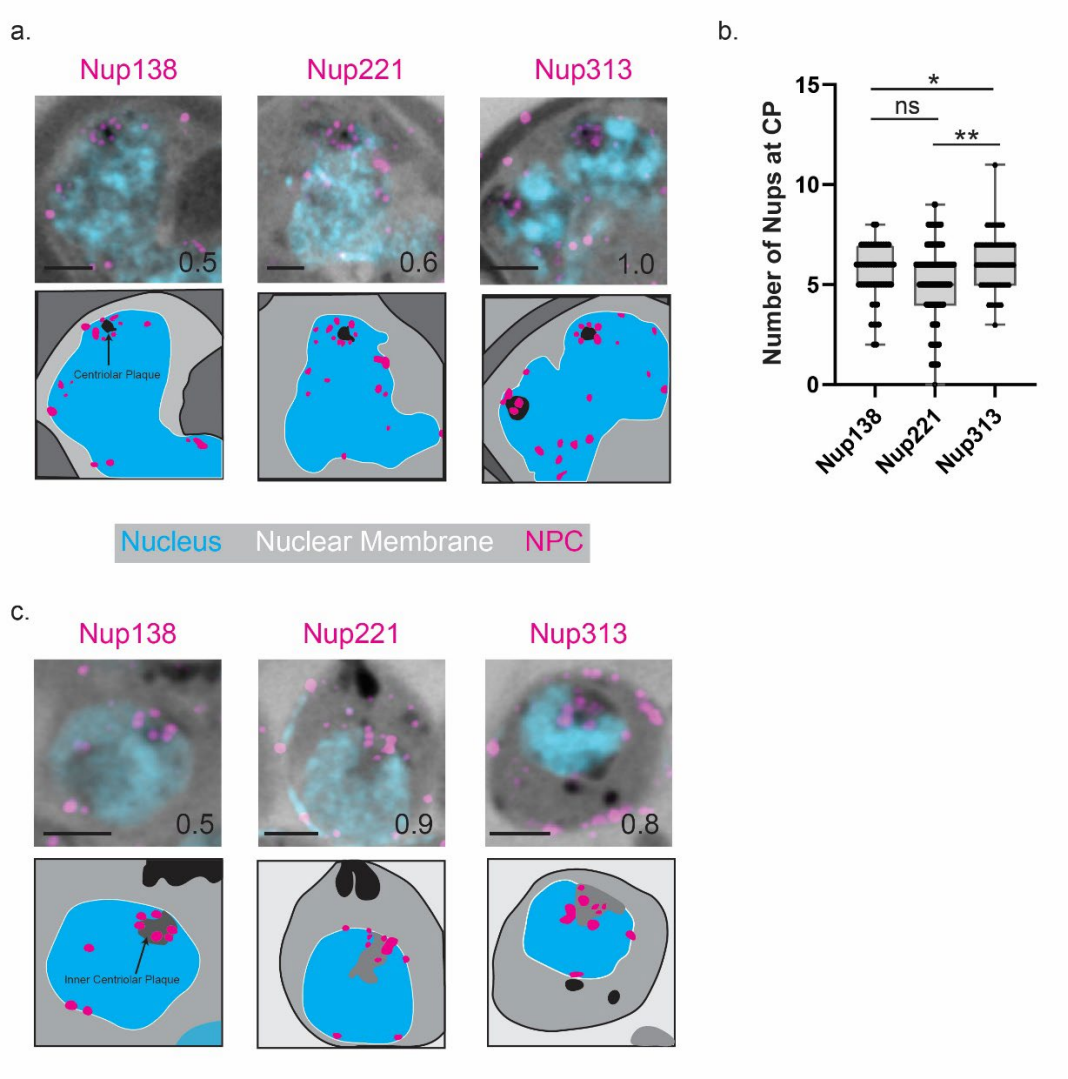


**Fig. 4: P. berghei NPCs organize around the centriolar plaque (CP) during and after mitosis. a.** Representative images of mitotic nuclei containing CPs (indicated by black staining of NHS ester) and the organization of three respective FG Nups around the CP. Nups are shown in magenta, DNA is shown in blue, protein density is shown in grayscale. **b.** Quantitation of Nups around the CPs in Nup138-smHA, Nup221-3xHA/GFP, and Nup313-smHA stained NPCs. * indicates P-value > 0.05, ** indicates P-value >0.005. **c.** Representative images of post-mitotic CPs and the organization of three respective FG Nups around where the inner CP disassembles. Nups are shown in magenta, DNA is shown in blue, protein density is shown in grayscale Scale bars 2 µm, image depth in µm indicated on the image.

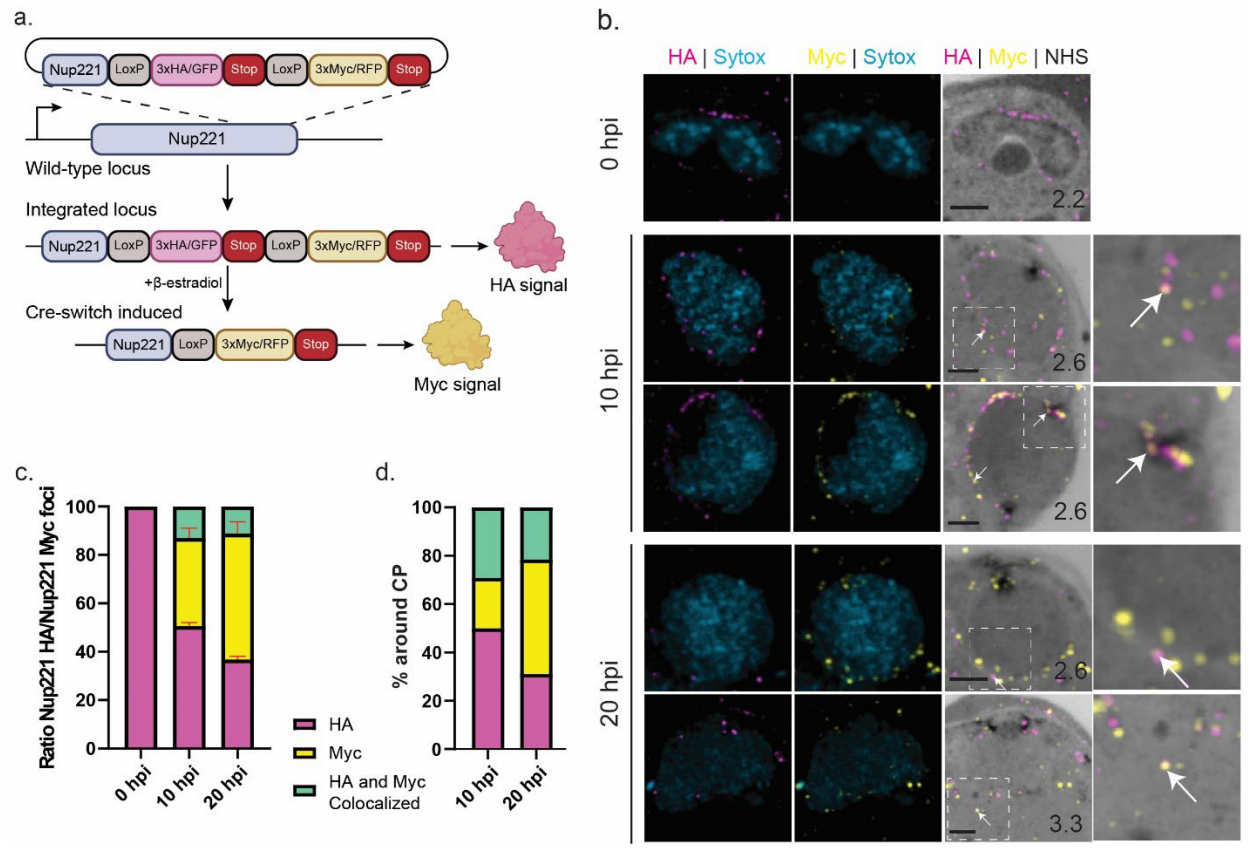


**Fig. 5: *P. berghei* replaces Nups in post-first mitotic NPCs.**

**a.** Schematic showing endogenous tagging strategy to introduce the RITE system at the 3' end of the *Nup221* gene. Translocation of Cre-EBD to the nucleus following treatment with β-estradiol results in excision between loxP sites, removing the original 3xHA/GFP tag while bringing the 3xMyc/RFP tag into frame. **b.** Representative images of *P. berghei* parasites at 0 hours post, 10 hours post, and 20 hours post induction with β-estradiol. HA signal (Scale bars 2 µm, Image depth in µm indicated. White arrows indicate areas of colocalization between HA and Myc. **c.** Ratio Nup221-HA/Nup221-Myc foci in 0 hours-, 10 hours- and 20 hours post induction with β-estradiol. Green bars indicate number of foci that had both HA and Myc signal. **d.** Amount of HA or Myc signal found around the CP in 10 hour- and 20 hour post induction parasites determined by counting foci around the CP. Green bars indicate foci containing both HA and Myc signal.

431 **Methods:**

432 **Parasite maintenance**

433 *P. berghei* ANKA clone 2.34 and derivatives were maintained in Swiss Webster mice
434 (Charles River). All experiments involving rodents were reviewed and approved by the Iowa State
435 University Institutional Animal Care and Use Committee.

436 **Genetic modification of *Plasmodium berghei***

437 Plasmid cloning was carried out using NEBuilder HIFI DNA assembly (NEB). Primer
438 sequences are given in Table 1. To generate a smHA (Viswanathan, Williams et al. 2015) fusion
439 at the endogenous C terminus of *P. berghei* Nup138 the smHA coding sequence was amplified
440 from plasmid pCAG_smFP_HA(Addgene #59759) using primers P4121/4122 and inserted
441 between BamHI/BsiWI immediately downstream of the *Pbnup138* homology region in the
442 plasmid pLIS0654 (Ambekar Sushma, Beck Josh et al. 2022) resulting in the plasmid pSA026. To
443 generate a smHA fusion at the endogenous C terminus of *P. berghei* Nup313, a homology region
444 corresponding to the 3' coding sequence of *Pbnup313* up to but not including the stop codon was
445 amplified with primers P4140/4126 from *P. berghei* genomic DNA and inserted between
446 AvrII/BamHI in pSA026, replacing the *Pbnup138* homology region and resulting in the plasmid
447 pSA028.

448 To generate parasites expressing Cre-EBD with the RITE cassette fused to the endogenous
449 C terminus of *P. berghei* Nup221, the Cre-EBD coding sequence was amplified from the plasmid
450 pTWO40 (Terweij, van Welsem et al. 2013) (Addgene #64769) and the RITE cassette was
451 amplified from the plasmid pKV016, which includes a 3xHA-GFP fusion in the pre-excised state
452 and a 3xMYC-mRFP fusion in the post-excised state (Menendez-Benito, van Deventer et al. 2013)
453 (Addgene #64767). These sequences were assembled together with a *Pbnup221* homology
454 region (Ambekar Sushma, Beck Josh et al. 2022), placing Cre-EBD under the control of *P. berghei*
455 EF1 alpha promoter and the hDHFR selectable marker under the control of the *P. berghei* EF1
456 delta promoter and positioning the hDHFR cassette between the two loxP-containing RITE tags

457 to facilitate marker removed upon excision. The mRFP sequence in the post-excision RITE fusion
458 was subsequently replaced with mRuby3 to yield the final plasmid pL857.

459 Plasmids pSA026, pSA028 and pL857 were linearized within the *Pbnup138*, *Pbnup313 or*
460 *Pbnup221* homology region using HindIII, PacI or ScaI, respectively, and transfected into *P.*
461 *berghei* as described (Hussain, Linera-Gonzalez et al. 2022). Transfected parasites were injected
462 into naïve mice and selected with 0.07 mg/ml pyrimethamine provided *ad libitum* in drinking
463 water beginning 24 hours post-transfection. Parasites were genotyped to confirm integration at
464 *Pbnup138*, *Pbnup313* or *Pbnup221* using PCR strategies described in Supplementary Figures 2
465 and 4.

466 **Live imaging and immunofluorescence assays**

467 For live imaging of parasites at regular intervals throughout the experiment, 100µl
468 parasite culture was spun down and resuspended in PBS containing 1µg/ml Hoechst 33342 to
469 stain nuclei. Following a brief incubation at 37℃, parasites were imaged with a 63x objective on
470 an Axio Observer 7 equipped with an Axiocam 702 mono camera and Zen 2.6 Pro software (Zeiss)
471 using the same exposure times for all images across sample groups and experimental
472 replicates.For immunofluorescence assays on unexpanded cells, thin blood smears were air dried
473 and fixed in ice-cold methanol/acetone (50:50) (for detection of smHA tagged Nup138, Nup313
474 or for detection of Cre). Fixed slides were blocked with Rockland blocking buffer (Rockland) and
475 probed with the primary and secondary antibodies indicated below. ,Slides were mounted in
476 Fluoromount-G with DAPI (Invitrogen).

477 **Ultrastructure expansion microscopy**

478 Ultrastructure expansion microscopy was performed as previously described on fixed
479 samples. Briefly, parasites were fixed in 4% PFA/PBS supplemented with 0.0075% glutaraldehyde
480 by the lab of Dr. Josh Beck at Iowa State University and were sent to the lab of Dr. Sabrina Absalon
481 at Indiana University School of Medicine. 12 mm round coverslips (Fisher Cat. No. NC1129240)
482 were treated with poly-D-lysine for 1 hour at 37 °C, washed three times with MilliQ water, and

483 placed in the wells of a 24-well dish. Fixed samples were resuspended at roughly 1.0 % hematocrit
484 in 1xPBS and 500 µL of parasite sample was added to the wells containing the coated coverslips
485 for 30 minutes at 37 °C. Following parasites settling, coverslips were washed 3 times in 1xPBS
486 before treating with 500 µL 1.4% v/v formaldehyde/2% v/v acylamide (FA/AA) in PBS. Samples
487 were incubated overnight at 37 °C. Gelation, denaturation, staining, and expansion of the gels
488 were performed as previously described (Liffner and Absalon 2021). Stained gels were imaged
489 using a Zeiss LSM900 AxioObserver with an Airyscan 2 detector. Images were taken using a 63x
490 Plan-Apochromat objective lens with a numerical aperature of 1.4.

491 **RITE experiment setup**

492 Asynchronous Nup221::RITE *P. berghei* parasites were collected and allowed to develop
493 overnight in vitro into terminal schizonts. Schizonts were magnetically purified on a MACS LD
494 column (Miltenyi Biotec) and IV injected into naïve mice to establish a synchronous infection.
495 Infections were allowed to develop for three intraerythrocytic developmental cycles (IDCs) to
496 increase parasitemia, then collected at 72 hpi when parasites were predominantly ring stage and
497 passed through a MACS LD column to remove any trophozoites or schizonts by collecting the flow
498 through.

499 These synchronized ring-stage parasites were used to establish in vitro cultures in
500 complete RPMI containing 200nM β-estradiol or DMSO (vehicle control). Parasites were collected
501 every two hours for live imaging and genomic DNA isolation. After 24 hours, parasites were
502 washed to remove β-estradiol or DMSO and IV injected into naïve mice to monitor Nup turnover
503 in subsequent IDCs. Mice were not provided with pyrimethamine to avoid killing parasites that
504 had undergone excision, which also removes the hDHFR selection marker.

505 **Antibodies and stains**

506 The following antibodies were used for widefield IFA analysis: rabbit polyclonal anti-HA
507 (1:500, Thermofisher SG77), rabbit anti-Cre polyclonal (1:500, Abcam ab190177). The following
508 antibodies were used for the preparation of stained gels for expansion microscopy: Rat anti-HA

509 (3F10, 1:25, Roche 12158167001), Mouse IgG1 anti-alpha Tubulin Clone B-5-1-2 (1:500,
510 ThermoFisher 32-2500), Rabbit anti-Myc polyclonal (1:500, ThermoFisher 710007). Goat anti-
511 rabbit Alexa Fluor 594 (1:500, ThermoFisher A11012), Goat anti-rat Alexa Fluor 488 (1:500,
512 ThermoFisher A1106), Goat anti-mouse IgG(H+L) Alexa Fluor 555 (1:500, ThermoFisher A21422),
513 and Goat anti-rabbit Alexa Fluor 555 (1:500, ThermoFisher A32732) were used as secondary
514 antibodies. NHS Ester Alexa Fluor 405 in DMSO (8 µg/mL, ThermoFisher A30000) was used to
515 stain proteins and SYTOX™ Deep Red (1 µM, ThermoFisher S11380) was used as a DNA stain.

516 **Image analysis**

517 All image analysis was done using 3D Airyscan processing at moderate filter strength on
518 Zen Blue Version 3.1 (Zeiss, Oberkochen, Germany). Images shown in this manuscript are
519 maximum intensity projections of between 5 and 60 z-slices of the entire image, with the number
520 indicated as the total Z-depth of the image (Z depth = 0.13 µm * number of slices taken for
521 projection)

522 **Statistical analysis**

523 Graphical data and statistical analysis was performed on Graphpad Prism version 9.0.

524 **Acknowledgements**

525 We thank The Company of Biologists Travelling Fellowship grant JCSTF2202676 (S.V.A)
526 for initial travel funding to begin this project. This work was supported by NIH grant AI139579
527 (G.R.M. and J.R.B.) and was made possible by an award from the Indiana University School of
528 Medicine (S.A., BRG award #2286272). The content is solely the responsibility of the authors
529 and does not necessarily represent the official views of the Indiana University School of
530 Medicine.

531 **Competing interests**

532 The authors declare no competing financial interests.

533 **Author Contributions:**

534 **Conceptualization:** J.B., S.V.A., G.R.M., J.R.B., and S.A.; **Methodology:** J.B., S.V.A., G.R.M., J.R.B.,
535 and S.A.; **Investigation:** J.B., S.V.A., and T.H.; **Data Analysis:** J.B., S.A. **Writing – Original Draft:**
536 J.B.; **Writing – Review and Editing:** J.B., S.V.A., T.H., G.R.M., J.R.B., and S.A; **Funding Acquisition:**
537 S.V.A., G.R.M., J.R.B., and S.A.; **Supervision:** G.R.M., J.R.B. and S.A.

538 **References:**


539 Allegretti, M., C. E. Zimmerli, V. Rantos, F. Wilfling, P. Ronchi, H. K. H. Fung, C.-W. Lee, W. Hagen, B.
540 Turoňová, K. Karius, M. Börmel, X. Zhang, C. W. Müller, Y. Schwab, J. Mahamid, B. Pfander, J. Kosinski and
541 M. Beck (2020). "In-cell architecture of the nuclear pore and snapshots of its turnover." Nature
542 **586**(7831): 796-800.
543
544 Ambekar Sushma, V., R. Beck Josh and R. Mair Gunnar (2022). "TurboID Identification of Evolutionarily
545 Divergent Components of the Nuclear Pore Complex in the Malaria Model Plasmodium berghei." mBio
546 **13**(5): e01815-01822.
547
548 Arnot, D. E., E. Ronander and D. C. Bengtsson (2011). "The progression of the intra-erythrocytic cell cycle
549 of Plasmodium falciparum and the role of the centriolar plaques in asynchronous mitotic division during
550 schizogony." Int J Parasitol **41**(1): 71-80.
551
552 Beck, M. and E. Hurt (2017). "The nuclear pore complex: understanding its function through structural
553 insight." Nature Reviews Molecular Cell Biology **18**(2): 73-89.
554
555 Bertiaux, E., A. C. Balestra, L. Bournonville, V. Louvel, B. Maco, D. Soldati-Favre, M. Brochet, P. Guichard
556 and V. Hamel (2021). "Expansion microscopy provides new insights into the cytoskeleton of malaria
557 parasites including the conservation of a conoid." PLoS Biol **19**(3): e3001020.
558
559 Bushell, E., A. R. Gomes, T. Sanderson, B. Anar, G. Girling, C. Herd, T. Metcalf, K. Modrzynska, F. Schwach,
560 R. E. Martin, M. W. Mather, G. I. McFadden, L. Parts, G. G. Rutledge, A. B. Vaidya, K. Wengelnik, J. C.
561 Rayner and O. Billker (2017). "Functional Profiling of a Plasmodium Genome Reveals an Abundance of
562 Essential Genes." Cell **170**(2): 260-272.e268.
563
564 Caroline, S. S., F. Charlotta, B. Johanna, V. Yannik, M. Marta, P. Alexander, K. Darius, C. Marek, K. Juyeop,
565 G. Markus and G. Julien (2021). "An extended DNA-free intranuclear compartment organizes centrosome
566 microtubules in malaria parasites." Life Science Alliance **4**(11): e202101199.
567
568 Chial, H. J., M. P. Rout, T. H. Giddings and M. Winey (1998). "Saccharomyces cerevisiae Ndc1p is a shared
569 component of nuclear pore complexes and spindle pole bodies." J Cell Biol **143**(7): 1789-1800.
570
571 Colombi, P., B. M. Webster, F. Fröhlich and C. P. Lusk (2013). "The transmission of nuclear pore complexes
572 to daughter cells requires a cytoplasmic pool of Nsp1." Journal of Cell Biology **203**(2): 215-232.
573

574 Courjol, F., T. Mouveaux, K. Lesage, J. M. Saliou, E. Werkmeister, M. Bonabaud, M. Rohmer, C. Slomianny,
575 F. Lafont and M. Gissot (2017). "Characterization of a nuclear pore protein sheds light on the roles and
576 composition of the Toxoplasma gondii nuclear pore complex." Cell Mol Life Sci **74**(11): 2107-2125.
577
578 Dahan-Pasternak, N., A. Nasereddin, N. Kolevzon, M. Pe'er, W. Wong, V. Shinder, L. Turnbull, C. B.
579 Whitchurch, M. Elbaum, T. W. Gilberger, E. Yavin, J. Baum and R. Dzikowski (2013). "PfSec13 is an unusual
580 chromatin-associated nucleoporin of Plasmodium falciparum that is essential for parasite proliferation in
581 human erythrocytes." Journal of Cell Science **126**(14): 3055-3069.
582
583 Degrasse, J. A. and D. Devos (2010). "A functional proteomic study of the Trypanosoma brucei nuclear
584 pore complex: an informatic strategy." Methods Mol Biol **673**: 231-238.
585
586 Devos, D., S. Dokudovskaya, R. Williams, F. Alber, N. Eswar, B. T. Chait, M. P. Rout and A. Sali (2006).
587 "Simple fold composition and modular architecture of the nuclear pore complex." Proc Natl Acad Sci U S
588 A **103**(7): 2172-2177.
589
590 Dey, G. and B. Baum (2021). "Nuclear envelope remodelling during mitosis." Curr Opin Cell Biol **70**: 67-
591 74.
592
593 Dey, G., S. Culley, S. Curran, U. Schmidt, R. Henriques, W. Kukulski and B. Baum (2020). "Closed mitosis
594 requires local disassembly of the nuclear envelope." Nature **585**(7823): 119-123.
595
596 Doye, V., R. Wepf and E. C. Hurt (1994). "A novel nuclear pore protein Nup133p with distinct roles in
597 poly(A)+ RNA transport and nuclear pore distribution." The EMBO Journal **13**(24): 6062-6075.
598
599 Fernandes, P., S. Briquet, D. Patarot, M. Loubens, B. Hoareau-Coudert and O. Silvie (2020). "The
600 dimerisable Cre recombinase allows conditional genome editing in the mosquito stages of Plasmodium
601 berghei." PLoS One **15**(10): e0236616.
602
603 Ferreira, J., J. H. Stear and H. Saumweber (2017). "Nucleoporins NPP-10, NPP-13 and NPP-20 are
604 required for HCP-4 nuclear import to establish correct centromere assembly." J Cell Sci **130**(5): 963-974.
605
606 Ferreira, J. L., V. Pražák, D. Vasishtan, M. Siggel, F. Hentzschel, A. M. Binder, E. Pietsch, J. Kosinski, F.
607 Frischknecht, T. W. Gilberger and K. Grünewald (2023). "Variable microtubule architecture in the malaria
608 parasite." Nat Commun **14**(1): 1216.
609
610 Gambarotto, D., F. U. Zwettler, M. Le Guennec, M. Schmidt-Cernohorska, D. Fortun, S. Borgers, J. Heine, J.
611 G. Schloetel, M. Reuss, M. Unser, E. S. Boyden, M. Sauer, V. Hamel and P. Guichard (2019). "Imaging
612 cellular ultrastructures using expansion microscopy (U-ExM)." Nat Methods **16**(1): 71-74.
613
614 Gerald, N., B. Mahajan and S. Kumar (2011). "Mitosis in the human malaria parasite Plasmodium
615 falciparum." Eukaryotic cell **10**(4): 474-482.
616
617 Gomar-Alba, M. and M. Mendoza (2020). "Modulation of Cell Identity by Modification of Nuclear Pore
618 Complexes." Frontiers in Genetics **10**.
619

620 Gomes, A. R., E. Bushell, F. Schwach, G. Girling, B. Anar, M. A. Quail, C. Herd, C. Pfander, K. Modrzynska, J.
621 C. Rayner and O. Billker (2015). "A genome-scale vector resource enables high-throughput reverse
622 genetic screening in a malaria parasite." Cell Host Microbe **17**(3): 404-413.
623
624 Grossman, E., O. Medalia and M. Zwerger (2012). "Functional Architecture of the Nuclear Pore
625 Complex." Annual Review of Biophysics **41**(1): 557-584.
626
627 Hinshaw, J. E. and R. A. Milligan (2003). "Nuclear pore complexes exceeding eightfold rotational
628 symmetry." Journal of Structural Biology **141**(3): 259-268.
629
630 Hinterndorfer, K., M. H. Laporte, F. Mikus, L. Tafur, C. Bourgoint, M. Prouteau, G. Dey, R. Loewith, P.
631 Guichard and V. Hamel (2022). "Ultrastructure expansion microscopy reveals the cellular architecture of
632 budding and fission yeast." Journal of Cell Science **135**(24): jcs260240.
633
634 Hoelz, A., E. W. Debler and G. Blobel (2011). "The Structure of the Nuclear Pore Complex." Annual
635 Review of Biochemistry **80**(1): 613-643.
636
637 Hussain, T., J. Linera-Gonzalez, J. M. Beck, M. A. Fierro, G. R. Mair, R. C. Smith and J. R. Beck (2022). "The
638 PTEX Pore Component EXP2 Is Important for Intrahepatic Development during the Plasmodium Liver
639 Stage." mBio **13**(6): e0309622.
640
641 Jaspersen, S. L. and S. Ghosh (2012). "Nuclear envelope insertion of spindle pole bodies and nuclear pore
642 complexes." Nucleus **3**(3): 226-236.
643
644 Kane, M., S. V. Rebensburg, M. A. Takata, T. M. Zang, M. Yamashita, M. Kvaratskhelia and P. D. Bieniasz
645 (2018). "Nuclear pore heterogeneity influences HIV-1 infection and the antiviral activity of MX2." eLife **7**:
646 e35738.
647
648 Kehrer, J., C. Kuss, A. Andres-Pons, A. Reustle, N. Dahan, D. Devos, M. Kudryashev, M. Beck, G. R. Mair
649 and F. Frischknecht (2018). "Nuclear Pore Complex Components in the Malaria Parasite Plasmodium
650 berghei." Scientific Reports **8**(1): 11249.
651
652 Kent, R. S., K. K. Modrzynska, R. Cameron, N. Philip, O. Billker and A. P. Waters (2018). "Inducible
653 developmental reprogramming redefines commitment to sexual development in the malaria parasite
654 Plasmodium berghei." Nat Microbiol **3**(11): 1206-1213.
655
656 Kutay, U., R. Jühlen and W. Antonin (2021). "Mitotic disassembly and reassembly of nuclear pore
657 complexes." Trends in Cell Biology **31**(12): 1019-1033.
658
659 Lee, C.-W., F. Wilfling, P. Ronchi, M. Allegretti, S. Mosalaganti, S. Jentsch, M. Beck and B. Pfander (2020).
660 "Selective autophagy degrades nuclear pore complexes." Nature Cell Biology **22**(2): 159-166.
661
662 Lénárt, P., G. Rabut, N. Daigle, A. R. Hand, M. Terasaki and J. Ellenberg (2003). "Nuclear envelope
663 breakdown in starfish oocytes proceeds by partial NPC disassembly followed by a rapidly spreading
664 fenestration of nuclear membranes." J Cell Biol **160**(7): 1055-1068.
665

666 Liffner, B. and S. Absalon (2021) "Expansion Microscopy Reveals Plasmodium falciparum Blood-Stage
667 Parasites Undergo Anaphase with A Chromatin Bridge in the Absence of Mini-Chromosome Maintenance
668 Complex Binding Protein." Microorganisms **9** DOI: 10.3390/microorganisms9112306.
669
670 Liffner, B., A. K. Cepeda Diaz, J. Blauwkamp, D. Anaguano, S. Frölich, V. Muralidharan, D. W. Wilson, J.
671 Dvorin and S. Absalon (2023). Atlas of Plasmodium falciparum intraerythrocytic development using
672 expansion microscopy, eLife Sciences Publications, Ltd.
673
674 Lin, D. H. and A. Hoelz (2019). "The Structure of the Nuclear Pore Complex (An Update)." Annu Rev
675 Biochem **88**: 725-783.
676
677 Linder, M. I., M. Köhler, P. Boersema, M. Weberruss, C. Wandke, J. Marino, C. Ashiono, P. Picotti, W.
678 Antonin and U. Kutay (2017). "Mitotic Disassembly of Nuclear Pore Complexes Involves CDK1- and PLK1-
679 Mediated Phosphorylation of Key Interconnecting Nucleoporins." Dev Cell **43**(2): 141-156.e147.
680
681 Menendez-Benito, V., S. J. van Deventer, V. Jimenez-Garcia, M. Roy-Luzarraga, F. van Leeuwen and J.
682 Neefjes (2013). "Spatiotemporal analysis of organelle and macromolecular complex inheritance." Proc
683 Natl Acad Sci U S A **110**(1): 175-180.
684
685 Neumann, N., D. Lundin and A. M. Poole (2010). "Comparative genomic evidence for a complete nuclear
686 pore complex in the last eukaryotic common ancestor." PLoS One **5**(10): e13241.
687
688 Ori, A., N. Banterle, M. Iskar, A. Andrés-Pons, C. Escher, H. Khanh Bui, L. Sparks, V. Solis-Mezarino, O.
689 Rinner, P. Bork, E. A. Lemke and M. Beck (2013). "Cell type-specific nuclear pores: a case in point for
690 context-dependent stoichiometry of molecular machines." Mol Syst Biol **9**: 648.
691
692 Otsuka, S. and J. Ellenberg (2018). "Mechanisms of nuclear pore complex assembly – two different ways
693 of building one molecular machine." FEBS Letters **592**(4): 475-488.
694
695 Powers, M. A., D. J. Forbes, J. E. Dahlberg and E. Lund (1997). "The vertebrate GLFG nucleoporin, Nup98,
696 is an essential component of multiple RNA export pathways." J Cell Biol **136**(2): 241-250.
697
698 Pulianmackal, A. J., K. Kanakousaki, K. Flegel, O. G. Grushko, E. Gourley, E. Rozich and L. A. Buttitta
699 (2022). "Misregulation of Nucleoporins 98 and 96 leads to defects in protein synthesis that promote
700 hallmarks of tumorigenesis." Dis Model Mech **15**(3).
701
702 Simon, C. S., C. Funaya, J. Bauer, Y. Voβ, M. Machado, A. Penning, D. Klaschka, M. Cyrklaff, J. Kim, M.
703 Ganter and J. Guizetti (2021). "An extended DNA-free intranuclear compartment organizes centrosome
704 microtubules in malaria parasites." Life Sci Alliance **4**(11).
705
706 Strawn, L. A., T. Shen, N. Shulga, D. S. Goldfarb and S. R. Wente (2004). "Minimal nuclear pore complexes
707 define FG repeat domains essential for transport." Nature Cell Biology **6**(3): 197-206.
708
709 Terweij, M., T. van Welsem, S. van Deventer, K. F. Verzijlbergen, V. Menendez-Benito, D. Ontoso, P. San-
710 Segundo, J. Neefjes and F. van Leeuwen (2013). "Recombination-induced tag exchange (RITE) cassette
711 series to monitor protein dynamics in Saccharomyces cerevisiae." G3 (Bethesda) **3**(8): 1261-1272.
712

713 Tomioka, Y., T. Kotani, H. Kirisako, Y. Oikawa, Y. Kimura, H. Hirano, Y. Ohsumi and H. Nakatogawa (2020).
714 "TORC1 inactivation stimulates autophagy of nucleoporin and nuclear pore complexes." J Cell Biol
715 **219**(7).
716
717 Toyama, B. H., R. Arrojo e Drigo, V. Lev-Ram, R. Ramachandra, T. J. Deerinck, C. Lechene, M. H. Ellisman
718 and M. W. Hetzer (2018). "Visualization of long-lived proteins reveals age mosaicism within nuclei of
719 postmitotic cells." Journal of Cell Biology **218**(2): 433-444.
720
721 Unwin, P. N. and R. A. Milligan (1982). "A large particle associated with the perimeter of the nuclear pore
722 complex." Journal of Cell Biology **93**(1): 63-75.
723
724 Verzijlbergen, K. F., V. Menendez-Benito, T. van Welsem, S. J. van Deventer, D. L. Lindstrom, H. Ovaa, J.
725 Neefjes, D. E. Gottschling and F. van Leeuwen (2010). "Recombination-induced tag exchange to track old
726 and new proteins." Proceedings of the National Academy of Sciences **107**(1): 64-68.
727
728 Viswanathan, S., M. E. Williams, E. B. Bloss, T. J. Stasevich, C. M. Speer, A. Nern, B. D. Pfeiffer, B. M.
729 Hooks, W. P. Li, B. P. English, T. Tian, G. L. Henry, J. J. Macklin, R. Patel, C. R. Gerfen, X. Zhuang, Y. Wang, G.
730 M. Rubin and L. L. Looger (2015). "High-performance probes for light and electron microscopy." Nat
731 Methods **12**(6): 568-576.
732
733 Weiner, A., N. Dahan-Pasternak, E. Shimoni, V. Shinder, P. von Huth, M. Elbaum and R. Dzikowski (2011).
734 "3D nuclear architecture reveals coupled cell cycle dynamics of chromatin and nuclear pores in the
735 malaria parasite Plasmodium falciparum." Cellular Microbiology **13**(7): 967-977.
736
737 Winey, M., D. Yarar, T. H. Giddings and D. N. Mastronarde (1997). "Nuclear Pore Complex Number and
738 Distribution throughout theSaccharomyces cerevisiae Cell Cycle by Three-Dimensional Reconstruction
739 from Electron Micrographs of Nuclear Envelopes." Molecular Biology of the Cell **8**(11): 2119-2132.
740
741 Wu, X., L. H. Kasper, R. T. Mantcheva, G. T. Mantchev, M. J. Springett and J. M. A. van Deursen (2001).
742 "Disruption of the FG nucleoporin NUP98 causes selective changes in nuclear pore complex
743 stoichiometry and function." Proceedings of the National Academy of Sciences **98**(6): 3191-3196.
744
745 Zhang, M., C. Wang, T. D. Otto, J. Oberstaller, X. Liao, S. R. Adapa, K. Udenze, I. F. Bronner, D. Casandra,
746 M. Mayho, J. Brown, S. Li, J. Swanson, J. C. Rayner, R. H. Y. Jiang and J. H. Adams (2018). "Uncovering the
747 essential genes of the human malaria parasite Plasmodium falciparum by saturation mutagenesis."
748 Science **360**(6388).

749

750